

Scalable image-based visualization and alignment of spatial transcriptomics datasets

Highlights

- Interactive visualization of irregularly spaced spatial transcriptomics datasets
- Robust and efficient alignment of spatial transcriptomics datasets
- Easy-to-use GUI for automatic or manual section alignment
- Scalable and accessible software implementation

Authors

Stephan Preibisch,
Michael Innerberger,
Daniel León-Periñán, Nikos Karaiskos,
Nikolaus Rajewsky

Correspondence

preibischs@janelia.hhmi.org (S.P.),
nikolaos.karaiskos@mdc-berlin.de (N.K.),
rajewsky@mdc-berlin.de (N.R.)

In brief

Preibisch et al. present STIM, a robust, scalable, and interactive computational framework for aligning, visualizing, and working with spatial transcriptomics data that bridges the worlds of sequencing and image analysis. STIM builds on tried-and-tested computer vision algorithms to automatically create 3D volumes from serial sections with human-level accuracy.

Methods in Brief

Scalable image-based visualization and alignment of spatial transcriptomics datasets

Stephan Preibisch,^{1,6,7,*} Michael Innerberger,^{1,6} Daniel León-Periñán,² Nikos Karaiskos,^{2,*} and Nikolaus Rajewsky^{2,3,4,5,*}

¹Janelia Research Campus, Howard Hughes Medical Institute, Ashburn, VA, USA

²Max Delbrück Center for Molecular Medicine in the Helmholtz Association (MDC), Berlin Institute for Medical Systems Biology (BIMSB), Laboratory for Systems Biology of Gene Regulatory Elements, Berlin, Germany

³Humboldt-Universität zu Berlin, Institut für Biologie, 10099 Berlin, Germany

⁴DZHK (German Center for Cardiovascular Research), Partner Site Berlin, Berlin, Germany

⁵Department of Pediatric Oncology, Universitätsmedizin Charité, Berlin, Germany

⁶These authors have contributed equally

⁷Lead contact

*Correspondence: preibischs@janelia.hhmi.org (S.P.), nikolaos.karaiskos@mdc-berlin.de (N.K.), rajewsky@mdc-berlin.de (N.R.)

<https://doi.org/10.1016/j.cels.2025.101264>

SUMMARY

We present the “spatial transcriptomics imaging framework” (STIM), an imaging-based computational framework focused on visualizing and aligning high-throughput spatial sequencing datasets. STIM is built on the powerful, scalable `ImgLib2` and `BigDataViewer` (BDV) image data frameworks and thus enables novel development or transfer of existing computer vision techniques to the sequencing domain characterized by datasets with irregular measurement-spacing and arbitrary spatial resolution, such as spatial transcriptomics data generated by multiplexed targeted hybridization or spatial sequencing technologies. We illustrate STIM’s capabilities by representing, interactively visualizing, 3D rendering, automatically registering, and segmenting publicly available spatial sequencing data from 13 serial sections of mouse brain tissue and from 19 sections of a human metastatic lymph node. We demonstrate that the simplest alignment mode of STIM achieves human-level accuracy.

INTRODUCTION

Several recent technological breakthroughs have triggered the rapid development of numerous high-throughput spatial transcriptomics methods over the last few years. These fluorescent RNA hybridization-based^{1–5} or array-based RNA capture, barcoding, and subsequent sequencing^{6–13} techniques provide (typically at single-cell or subcellular resolution) molecular readouts within the native spatial context of a tissue, which is critical for understanding cellular interactions in healthy and diseased states.¹⁴ Therefore, the production of spatial transcriptomics datasets, already abundant and continuously expanding, is crucial for both basic life science research and clinical/medical applications. Handling and analysis of these datasets pose several complex challenges: (1) size—spatial sequencing generates several gigabytes of data for a single tissue section and we anticipate that to increase; (2) heterogeneity—datasets greatly differ in the number of genes and transcripts captured, their spatial resolution, and tissue architecture; (3) spatial transcriptomics data are, in contrast to image data, usually irregularly spaced; (4) three-dimensional (3D) integration—data from tissue sections need to be integrated into a 3D molecular map; (5) access and analyses—the need to easily share and interactively interrogate spatial transcriptomics data; and (6) flexibility and long-term availability—the need for open-source, community-based approaches.

Several methods have been developed to visualize, process, and align spatial transcriptomics data^{15–31}—each, however, having their own drawbacks. Here, we show that established methods from the computer vision field, which have been developed by a large scientific community for decades, can be adapted to meet challenges that the spatial transcriptomics field faces. Specifically, we present the “spatial transcriptomics imaging framework” (STIM), a computational, scalable, and extendable toolkit based on `ImgLib2`³² and `BigDataViewer`³³ that allows efficient handling, alignment and processing (including integration of 2D data into 3D molecular maps), visualization, and analysis of high-throughput spatial-omics datasets. We demonstrate the power of our approach by applying STIM to two distinct spatial sequencing datasets, integrating adjacent slices into 3D molecular maps for (1) 13 sections of an adult mouse brain and (2) 19 sections of a human metastatic lymph node. We additionally show how to use STIM to visualize the data and perform a simple, machine-learning-based segmentation task.

RESULTS

`ImgLib2`³² defines an image as a function f that maps coordinates C in n -dimensional space R^n to a value T

$$f : C \rightarrow T, C \subset R^n.$$

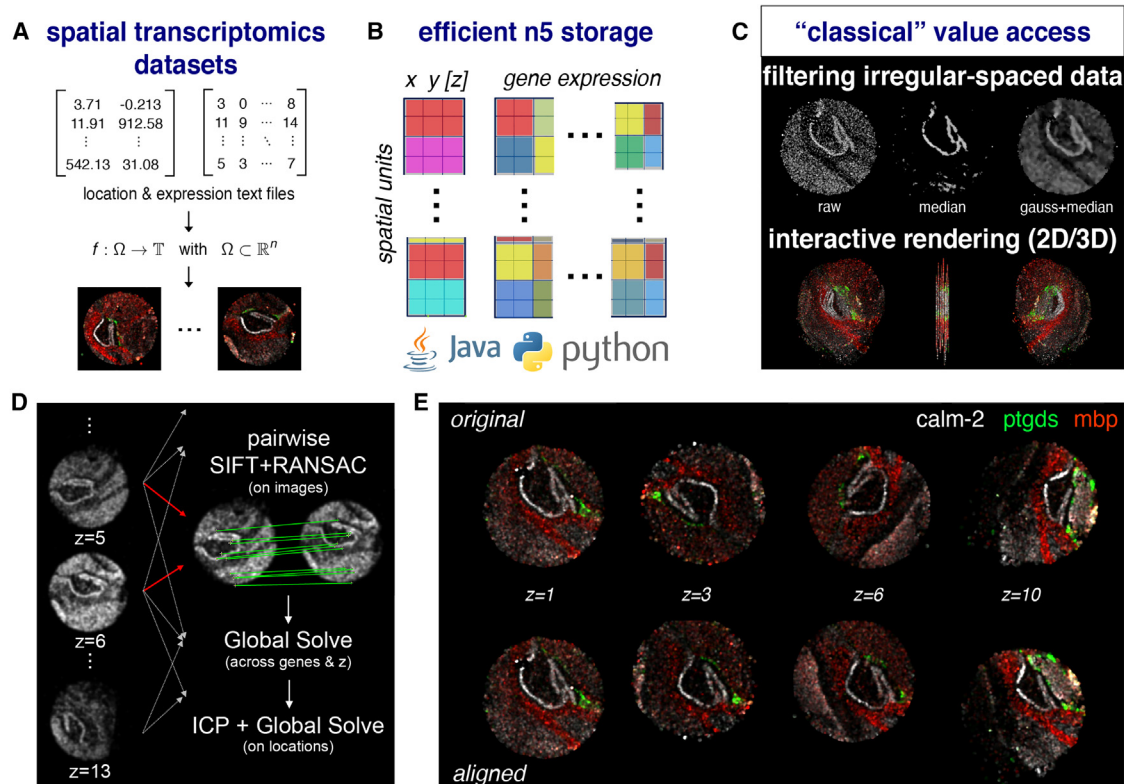


Figure 1. STIM applies state-of-the-art imaging techniques to store, align, visualize, and analyze massive amounts of spatial transcriptomics datasets

(A) Spatial transcriptomics datasets can be represented as images, with the number of genes per spatial unit corresponding to a number of different channels. (B) Expression and spatial data are stored in N5/ZARR containers for efficiency and scalability and are accessible within the provided Java and Python frameworks. (C) STIM provides classical value access operations such as filtering irregularly spaced data, resulting in smoothed gene expression or interactive rendering in 2D and 3D. (D) Schematic of how STIM aligns consecutive sections of spatial transcriptomics datasets. (E) Visualization of the spatial gene expression of three genes in four different sections of a published dataset. Top (bottom) row: spatial gene expression profiles in the original (aligned) puck orientations.

This definition illustrates that *ImgLib2* natively supports both regularly and irregularly spaced datasets (Figure S1). Furthermore, its generic, interface-driven design imposes no constraints on dataset size (biggest currently available implementation supports 4,096 petabyte), dimensionality, or data type, which is highlighted by the fact that many of the largest biological image datasets ever acquired^{34,35} were reconstructed using *ImgLib2*, the *ImgLib2*-backed BDV,³³ and the N5 (ZARR-compatible) file format (an open standard for storing large multi-dimensional data).³⁶ STIM builds on these frameworks to provide random, fast, and optionally distributed read&write access, interactive visualization, and efficient processing of spatial transcriptomics data.

STIM directly supports *AnnData* or re-saving of input datasets from the standardized text- or comma-separated formats into an N5/ZARR container (Figures 1A and 1B), while optionally log-normalizing the data. Coordinate- and gene-expression data can be loaded fast and memory-efficiently in blocks using the *ImgLib2*-cache framework, which can be accessed as values or as rendered images (Figures 1B and 1C). *ImgLib2* provides nearest-neighbor and linear interpolation for mapping irregularly

spaced samples onto pixel grids necessary for visualization. For a more realistic rendering at arbitrary resolutions, we implemented a rendering method based on Gaussian distributions (Figure 1, STAR Methods). Spatial image filtering, also referred to as digital filtering, is an established, powerful technique to enhance certain aspects of a signal that is represented as discrete samples (e.g., an image) using mathematical operations.³⁷ Although such filtering is mathematically directly applicable to irregularly spaced data, it is not widely available as efficient implementations require fast *k*-nearest neighbor search. To ease this barrier, we added a generic framework based on *ImgLib2* using *kd*-trees for applying filters (e.g., mean, median, or Gaussian) to irregularly spaced data that can easily be extended (Figure 1C). All operations are implemented virtually, allowing interactive access to and rendering of the data using BDV.

We demonstrate STIM's capabilities as follows. First, STIM can be used to filter the data and smoothen them, for instance, by applying a Median filter or others (Figure 1C; Videos S2 and S3). Second, tried-and-tested image registration techniques can be used to align datasets stemming from consecutive

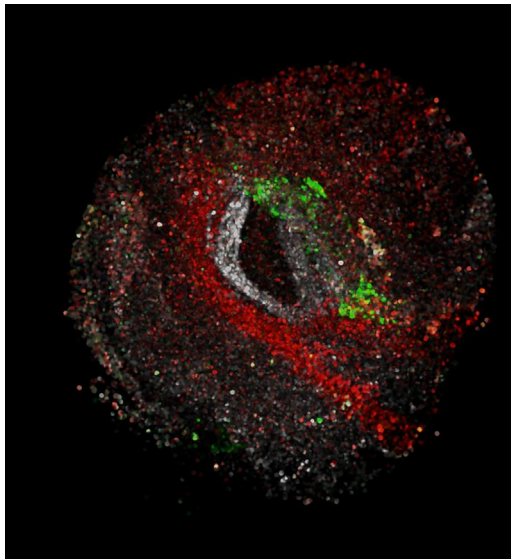


Figure 2. 3D rendering of the aligned Slide-seq dataset

The video shows gene *Calm2* in white, gene *Ptdgs* in green, and gene *Mbp* in red and highlights the 3D nature of the dataset after alignment when represented as a 3D image.

sections of the same tissue, as described below (Figures 1D and 1E; Video S2). Of note, we also developed a user-friendly, interactive BDV-based graphical user interface (GUI) for aligning pairs of tissue sections automatically or, optionally, manually using BDV transformation controls (Figure S7). Third, STIM offers an interactive visualization and exploration of the data through BDV in 2D and 3D, including the visualization of metadata—such as cell-type annotation—together with gene expression in every spatial unit (Figure S2, Video S3). Additionally, we show that existing machine-learning segmentation can be applied to spatial transcriptomics data and we highlight the applicability of existing 3D rendering methods (Figure 2/Video S1, STAR Methods).

Alignment

To illustrate the potential of applying computer vision techniques to sequencing datasets, we first aligned a series of consecutive brain hippocampus sections, which were published in Rodriques et al.,⁷ using STIM (Figure 2/Video S1). Each of these 2D sections contains between 12,000 and 33,000 cells and a median of ~50 quantified molecules at near-cellular resolution. To align the 13 sections in three dimensions, we adapt an alignment strategy originally developed for the registration of large electron and light microscopy datasets.^{38–40} We first apply scale invariant feature transform (SIFT)⁴¹ in combination with robust sample consensus (RANSAC)⁴² on rendered image pairs of sections (+2 in the z direction, Figure 1D). For each pair, we identify a set of corresponding points on a rigid 2D transformation across an automatically selected set of genes that show high entropy in both sections. To correctly identify as many corresponding points as possible, we run SIFT independently for each gene, with a low threshold for the minimal number of required points. RANSAC is then applied to all points of all genes again to identify those that agree on a common transformation across genes.

Next, we globally minimize the distance between all corresponding image points across all sections, yielding a single 2D transformation for each section (STAR Methods). In an optional refinement step, we use the iterative closest point (ICP) algorithm⁴³ on locations of sequenced spots rather than rendered images, where neighboring points within a predefined radius showing most similar expression values are assigned to be correspondences. Finally, using all ICP correspondences, we globally solve again and identify a regularized affine transformation model for each section that is stored in the N5/ZARR container. The resulting tissue dataset can be rendered in 3D using STIM (Figure 2/Video S1), and the STIM-explorer can be used to highlight the spatial expression of interactively selected genes on the whole tissue (Videos S2 and S3).

Due to the robustness of SIFT, our alignment pipeline can readily be employed across different technologies. Importantly, STIM was vital in constructing a 3D molecular map of a recently published human metastatic lymph node.¹³ This dataset consists of 19 non-consecutive sections and a total of >1.5 million cells. The pairwise and global alignment performed by STIM enabled the generation of the 3D virtual tissue block and the derivation of 3D-specific insights from the data.¹³ In another application, we used STIM to align six sections of human lung cancer tissue, each containing ~50,000 cells and being 30 μm apart.⁴⁴ Among other insights, the 3D molecular map in that case enabled the more precise identification of immune niches.⁴⁴

We further used STIM to align serial adult mouse brain sections produced with the Visium platform (Figure S3, Video S2). More generally, we anticipate STIM to process and stitch together consecutive tissue sections from the same tissue, regardless of the underlying spatial sequencing method. This enhances the information flow between the different sections and naturally enriches the molecular readouts.

The alignment pipeline we developed is based on linear transformations, typically affine transformation models regularized with rigid models. This allows the use of robust model estimation using RANSAC, which is also able to realize whether no proper alignment could be achieved. These potential gaps can be bridged using the interactive, manual alignment feature (Video S2). If the alignment quality needs to be further improved, existing non-rigid registration algorithms such as bUnwarpJ^{39,45} can be employed. However, it is important to realize that although deformations introduced by non-rigid transformations typically do improve the alignment quality (Figure S4), it is likely to deform the sample in an unnatural way. A simple example to visualize the problem is a cone in 3D, which would be represented as circles with increasing radius along the sections (in z). Non-rigid alignment would effectively transform these circles so that they show the same radius as it maximizes similarity, thus transforming the cone into a pipe. Therefore, meaningful and well-designed regularization is a necessity for employing non-rigid alignment, which has been well studied in image analysis^{39,45} but is, to the best of our knowledge, currently in its infancy for ST data.

Interoperability and accessibility

STIM is open source and leverages the large Java community built around ImgLib2. To enhance interoperability and enable the use of STIM by users who employ Python interfaces, we have added support for the popular AnnData format.⁴⁶ With

this support, it is possible to seamlessly access the data between the AnnData and the N5/ZARR formats, transferring the underlying sample metadata and facilitating downstream analyses. Moreover, STIM can be installed on Linux, MacOS, and Windows through the popular Conda packaging environment.

Benchmarking

Recently, several software packages for the alignment of spatial sequencing data have been developed specifically within the field of spatial transcriptomics (Table S1). Probabilistic alignment of spatial transcriptomics experiments (PASTE)⁴⁷ first solves an optimal transport problem to derive a probabilistic assignment of points for pairs of consecutive slices. Based on these, a rigid transformation model is sequentially estimated for each slice. Importantly, no optimization across slices is performed, which might prove problematic once dataset sizes increase (similar to the image-stitching problem), and *partial* alignment (i.e., sections only partially overlap in 2D) is not supported. More recently, PASTE³¹ introduced support for partial alignment, but the optimal transport framework is not scalable (in time or memory usage) to datasets with millions of cells. Furthermore, the computational complexity depends quadratically on the number of sequenced locations. Andersson et al.²³ rely on manual landmarks for alignment and also support only rigid transformation models. Jones et al.²⁴ and Qiu et al.²⁵ require an approximate initial alignment, using, for example, PASTE or STIM, and apply Gaussian process spatial alignment to extract warp functions for non-rigid alignment of consecutive slices, also at quadratic complexity with respect to the number of sequenced locations. Clifton et al.²⁶ require initialization via manual selection of corresponding points and do not offer global optimization across slices. Other methods rely on alignment of high-level features such as cell types or spatial regions, thus requiring extensive analysis of individual sections prior to alignment.^{27–29} Our proposed alternative approaches have been tried and tested in image analysis for decades and work reliably and fast on multi-terabyte images, while their complexity depends on the size of the rendered images, which can even be small for ST data. The complexity for transferring sequenced locations into images is equivalent to that of a kd-tree lookup, which is $O(\log n)$. The use of RANSAC for pairwise matching, global optimization with outlier removal across all pairwise results, and implementation in scalable frameworks *ImgLib2* and *BigDataViewer* ensure that the identified alignment can be trusted and that the approach will scale to significantly larger datasets in the future.

To quantitatively assess STIM's performance, we used the metastatic lymph node dataset comprising 19 sections. We performed five alignments using STIM's framework: one automatic, SIFT-based alignment of all sections and four manual alignments of all sections by four different individuals. Subsequently, we computed the pairwise distances between the transformed section pairs and across individuals and STIM (Figure S8A). The quality of STIM's automated alignment was found to be equivalent to human performance. By performing a grid search over STIM's parameters, we further validated that their effect on the quality of the alignment is only minimal (Figure S8B). The performance of publicly available methods was found to be lower (Figures S8C and S8D). Although SPACEL achieved similar average pairwise alignment quality to STIM, Morpho exhibited

higher alignment errors. However, both SPACEL and Morpho failed to produce accurate final 3D reconstructions due to error accumulation at partially overlapping sections, resulting in significant rotational misalignment between section groups (Figure S8E). Additionally, SPACEL requires cell-type annotations as input, and, hence, a pre-processing step, whereas STIM operates directly on raw data.

DISCUSSION

STIM enables efficient, distributed access, processing, and visualization of large-scale spatial transcriptomics datasets. Irregularly spaced data can be spatially filtered and accessed directly as values or rendered as images. STIM thereby acts as a bridge between the fields of computer vision and genomics, which we highlight by developing an automatic workflow for the alignment of sliced spatial transcriptomics datasets. Another application of STIM is to perform object segmentation on subcellular, high-resolution spatial transcriptomics datasets using existing image-based machine-learning solutions such as Random Forests (Figure S5)⁴⁸ or, for larger future datasets, StarDist⁴⁹ or CellPose.⁵⁰ We provide STIM as an extensible, open-source framework available on GitHub with interfaces in Java, Python, and on the command line. We believe that these properties of STIM have the potential to enable the community to further unite the worlds of image analysis and genomics.

RESOURCE AVAILABILITY

Lead contact

Requests for further information should be directed to the lead contact, Stephan Preibisch preibischs@janelia.hhmi.org.

Materials availability

Not applicable.

Data and code availability

All data analyzed within this work are publicly available. The datasets that were used for the alignment of mouse hippocampus sections were published in Slide-seq.⁷ The 10X Visium datasets were downloaded from the 10x Genomics website. The Open-ST data were downloaded from GEO (GEO: GSE251926).

All original code has been deposited at <https://github.com/PreibischLab/STIM> and <https://github.com/rajewsky-lab/stimwrap> and is publicly available. DOIs are listed in the key resources table (<https://doi.org/10.5281/zenodo.14911427> and <https://doi.org/10.5281/zenodo.14930579>).

Any additional information required to reanalyze the data reported in this paper is available from the lead contact upon request.

ACKNOWLEDGMENTS

S.P. was supported by the HFSP grant RGP0021/2018-102, MDC Berlin, and HHMI Janelia. M.I. was supported by HHMI Janelia. D.L.-P. was supported by the Helmholtz Einstein International Berlin Research School in Data Science (HEIBriDS) program of the Helmholtz Association. N.K. was supported by the DFG grants KA 5006/1-1 and RA 838/5-1. N.R. was supported by MDC Berlin and Charite. We thank the HHMI Janelia Open Science Software Initiative (OSSI, <https://ossi.janelia.org/>) for supporting this project.

DECLARATION OF INTERESTS

This work is part of a larger patent application in which N.K., S.P., and N.R. are among the inventors. The patent application (US20240257914A1) was

submitted through the Technology Transfer Office of the Max-Delbrück Center (MDC), with the MDC being the patent applicant.

STAR★METHODS

Detailed methods are provided in the online version of this paper and include the following:

- [KEY RESOURCES TABLE](#)
- [METHOD DETAILS](#)
 - Related software
 - N5 storage and normalization
 - Rendering of irregularly-spaced data
 - Filtering of irregularly-spaced data
 - Pairwise SIFT registration
 - Global Optimization
 - ICP refinement
- [QUANTIFICATION AND STATISTICAL ANALYSIS](#)
 - Benchmarking

SUPPLEMENTAL INFORMATION

Supplemental information can be found online at <https://doi.org/10.1016/j.cels.2025.101264>.

Received: July 12, 2024

Revised: January 24, 2025

Accepted: March 27, 2025

Published: April 22, 2025

REFERENCES

1. Lubeck, E., Coskun, A.F., Zhiyentayev, T., Ahmad, M., and Cai, L. (2014). Single-cell in situ RNA profiling by sequential hybridization. *Nat. Methods* *11*, 360–361. <https://doi.org/10.1038/nmeth.2892>.
2. Chen, K.H., Boettiger, A.N., Moffitt, J.R., Wang, S., and Zhuang, X. (2015). RNA imaging. Spatially resolved, highly multiplexed RNA profiling in single cells. *Science* *348*, aaa6090. <https://doi.org/10.1126/science.aaa6090>.
3. He, S., Bhatt, R., Brown, C., Brown, E.A., Buhr, D.L., Chantranuvatana, K., Danaher, P., Dunaway, D., Garrison, R.G., Geiss, G., et al. (2022). High-plex imaging of RNA and proteins at subcellular resolution in fixed tissue by spatial molecular imaging. *Nat. Biotechnol.* *40*, 1794–1806. <https://doi.org/10.1038/s41587-022-01483-z>.
4. Janesick, A., Shelansky, R., Gottscho, A.D., Wagner, F., Williams, S.R., Rouault, M., Belliakoff, G., Morrison, C.A., Oliveira, M.F., Sicherman, J.T., et al. (2023). High resolution mapping of the tumor microenvironment using integrated single-cell, spatial and in situ analysis. *Nat. Commun.* *14*, 8353. <https://doi.org/10.1038/s41467-023-43458-x>.
5. Groiss, S., Pabst, D., Faber, C., Meier, A., Bogdoll, A., Unger, C., Nilges, B., Strauss, S., Förderl-Höbenreich, E., Hardt, M., et al. (2021). Highly resolved spatial transcriptomics for detection of rare events in cells. Preprint at bioRxiv. <https://doi.org/10.1101/2021.10.11.463936>.
6. Ståhl, P.L., Salmén, F., Vickovic, S., Lundmark, A., Navarro, J.F., Magnusson, J., Giacomello, S., Asp, M., Westholm, J.O., Huss, M., et al. (2016). Visualization and analysis of gene expression in tissue sections by spatial transcriptomics. *Science* *353*, 78–82. <https://doi.org/10.1126/science.aaf2403>.
7. Rodrigues, S.G., Stickels, R.R., Goeva, A., Martin, C.A., Murray, E., Vanderburg, C.R., Welch, J., Chen, L.M., Chen, F., and Macosko, E.Z. (2019). Slide-seq: A scalable technology for measuring genome-wide expression at high spatial resolution. *Science* *363*, 1463–1467. <https://doi.org/10.1126/science.aaw1219>.
8. 10X Genomics Spatial Gene Expression – 10x Genomics. <https://www.10xgenomics.com/products/spatial-gene-expression>.
9. Cho, C.-S., Xi, J., Si, Y., Park, S.-R., Hsu, J.-E., Kim, M., Jun, G., Kang, H.M., and Lee, J.H. (2021). Microscopic examination of spatial transcriptome using Seq-Scope. *Cell* *184*, 3559–3572.e22. <https://doi.org/10.1016/j.cell.2021.05.010>.
10. Vickovic, S., Eraslan, G., Salmén, F., Klughammer, J., Stenbeck, L., Schapiro, D., Åjjö, T., Bonneau, R., Bergensträhle, L., Navarro, J.F., et al. (2019). High-definition spatial transcriptomics for in situ tissue profiling. *Nat. Methods* *16*, 987–990. <https://doi.org/10.1038/s41592-019-0548-y>.
11. Stickels, R.R., Murray, E., Kumar, P., Li, J., Marshall, J.L., Di Bella, D.J., Arlotta, P., Macosko, E.Z., and Chen, F. (2021). Highly sensitive spatial transcriptomics at near-cellular resolution with Slide-seqV2. *Nat. Biotechnol.* *39*, 313–319. <https://doi.org/10.1038/s41587-020-0739-1>.
12. Liu, Y., Yang, M., Deng, Y., Su, G., Enniful, A., Guo, C.C., Tebaldi, T., Zhang, D., Kim, D., Bai, Z., et al. (2020). High-Spatial-Resolution Multi-Omics Sequencing via Deterministic Barcoding in Tissue. *Cell* *183*, 1665–1681.e18. <https://doi.org/10.1016/j.cell.2020.10.026>.
13. Schott, M., León-Periñán, D., Splendiani, E., Strenger, L., Licha, J.R., Pentimalli, T.M., Schallenberg, S., Alles, J., Samut Tagliaferro, S., Boltengagen, A., et al. (2023). Open-ST: High-resolution spatial transcriptomics in. Preprint at bioRxiv. <https://doi.org/10.1101/2023.12.22.572554>.
14. Rao, A., Barkley, D., França, G.S., and Yanai, I. (2021). Exploring tissue architecture using spatial transcriptomics. *Nature* *596*, 211–220. <https://doi.org/10.1038/s41586-021-03634-9>.
15. Keller, M.S., Gold, I., McCallum, C., Manz, T., Kharchenko, P.V., and Gehlenborg, N. (2021). Vitessce: a framework for integrative visualization of multi-modal and spatially-resolved single-cell data. *Nat. Methods* *22*, 63–67. <https://doi.org/10.31219/osf.io/y8thv>.
16. Hao, Y., Hao, S., Andersen-Nissen, E., Mauck, W.M., Zheng, S., Butler, A., Lee, M.J., Wilk, A.J., Darby, C., Zager, M., et al. (2021). Integrated analysis of multimodal single-cell data. *Cell* *184*, 3573–3587.e29. <https://doi.org/10.1016/j.cell.2021.04.048>.
17. Palla, G., Spitzer, H., Klein, M., Fischer, D., Schaar, A.C., Kuemmerle, L.B., Rybakov, S., Ibarra, I.L., Holmberg, O., Virshup, I., et al. (2022). Squidpy: a scalable framework for spatial omics analysis. *Nat. Methods* *19*, 171–178. <https://doi.org/10.1038/s41592-021-01358-2>.
18. Fernández Navarro, J., Lundeberg, J., and Ståhl, P.L. (2019). ST viewer: a tool for analysis and visualization of spatial transcriptomics datasets. *Bioinformatics* *35*, 1058–1060. <https://doi.org/10.1093/bioinformatics/bty714>.
19. Schapiro, D., Jackson, H.W., Raghuraman, S., Fischer, J.R., Zanotelli, V.R.T., Schulz, D., Giesen, C., Catena, R., Varga, Z., and Bodenmiller, B. (2017). histoCAT: analysis of cell phenotypes and interactions in multiplex image cytometry data. *Nat. Methods* *14*, 873–876. <https://doi.org/10.1038/nmeth.4391>.
20. Dries, R., Zhu, Q., Dong, R., Eng, C.L., Li, H., Liu, K., Fu, Y., Zhao, T., Sarkar, A., Bao, F., et al. (2021). Giotto: a toolbox for integrative analysis and visualization of spatial expression data. *Genome Biol.* *22*, 78. <https://doi.org/10.1186/s13059-021-02286-2>.
21. Bergensträhle, J., Larsson, L., and Lundeberg, J. (2020). Seamless integration of image and molecular analysis for spatial transcriptomics workflows. *BMC Genomics* *21*, 482. <https://doi.org/10.1186/s12864-020-06832-3>.
22. Liu, X., Zeira, R., and Raphael, B.J. (2023). PASTE2: Partial Alignment of Multi-slice Spatially Resolved Transcriptomics Data. Preprint at bioRxiv. <https://doi.org/10.1101/2023.01.08.523162>.
23. Andersson, A., Andrusivová, Ž., Czarnewski, P., Li, X., Sundström, E., and Lundeberg, J. (2021). A Landmark-based Common Coordinate Framework for Spatial Transcriptomics Data. Preprint at bioRxiv. <https://doi.org/10.1101/2021.11.11.468178>.
24. Jones, A., Townes, F.W., Li, D., and Engelhardt, B.E. (2023). Alignment of spatial genomics data using deep Gaussian processes. *Nat. Methods* *20*, 1379–1387. <https://doi.org/10.1038/s41592-023-01972-2>.
25. Qiu, X., Zhu, D.Y., Yao, J., Jing, Z., Zuo, L., Wang, M., (Joseph) Min, K.H., Pan, H., Wang, S., Liao, S., et al. (2022). Spateo: multidimensional

- spatiotemporal modeling of single-cell spatial transcriptomics. Preprint at bioRxiv. <https://doi.org/10.1101/2022.12.07.519417>.
26. Clifton, K., Anant, M., Aihara, G., Atta, L., Aimiwu, O.K., Kebschull, J.M., Miller, M.I., Tward, D., and Fan, J. (2023). STalign: Alignment of spatial transcriptomics data using diffeomorphic metric mapping. *Nat. Commun.* *14*, 8123. <https://doi.org/10.1038/s41467-023-43915-7>.
 27. Yu, Y., and Xie, Z. (2024). Spatial Transcriptomic Alignment, Integration, and de novo 3D Reconstruction by STAIR. *Res. Sq.* <https://doi.org/10.21203/rs.3.rs-3939678/v1>.
 28. Xia, T., Hu, L., Zuo, L., Zhang, Y., Xu, M., Lu, Q., Zhang, L., Cao, L., Pan, T., Zhang, B., et al. (2023). ST-GEARS: Advancing 3D Downstream Research through Accurate Spatial Information Recovery. Preprint at BioRxiv. <https://doi.org/10.1101/2023.12.09.570320>.
 29. Xu, H., Wang, S., Fang, M., Luo, S., Chen, C., Wan, S., Wang, R., Tang, M., Xue, T., Li, B., et al. (2023). SPACEL: deep learning-based characterization of spatial transcriptome architectures. *Nat. Commun.* *14*, 7603. <https://doi.org/10.1038/s41467-023-43220-3>.
 30. Sztanka-Toth, T.R., Jens, M., Karaiskos, N., and Rajewsky, N. (2022). Spacemake: processing and analysis of large-scale spatial transcriptomics data. *GigaScience* *11*, giac064. <https://doi.org/10.1093/gigascience/giac064>.
 31. Liu, X., Zeira, R., and Raphael, B.J. (2023). Partial alignment of multislice spatially resolved transcriptomics data. *Genome Res.* *33*, 1124–1132. <https://doi.org/10.1101/gr.277670.123>.
 32. Pietzsch, T., Preibisch, S., Tomancák, P., and Saalfeld, S. (2012). ImgLib2—generic image processing in Java. *Bioinformatics* *28*, 3009–3011. <https://doi.org/10.1093/bioinformatics/bts543>.
 33. Pietzsch, T., Saalfeld, S., Preibisch, S., and Tomancak, P. (2015). BigDataViewer: visualization and processing for large image data sets. *Nat. Methods* *12*, 481–483. <https://doi.org/10.1038/nmeth.3392>.
 34. Scheffer, L.K., Xu, C.S., Januszewski, M., Lu, Z., Takemura, S.-Y., Hayworth, K.J., Huang, G.B., Shinomiya, K., Maitlin-Shepard, J., Berg, S., et al. (2020). A connectome and analysis of the adult *Drosophila* central brain. *eLife* *9*, e57443. <https://doi.org/10.7554/eLife.57443>.
 35. Gao, R., Asano, S.M., Upadhyayula, S., Pisarev, I., Milkie, D.E., Liu, T.-L., Singh, V., Graves, A., Huynh, G.H., Zhao, Y., et al. (2019). Cortical column and whole-brain imaging with molecular contrast and nanoscale resolution. *Science* *363*, eaau8302. <https://doi.org/10.1126/science.aau8302>.
 36. GitHub – saalfeldlab/n5: Not HDF5. <https://github.com/saalfeldlab/n5>.
 37. Oppenheim, A.V., and Schaffer, R.W. (1975). *Digital Signal Processing, First Edition* (Pearson).
 38. Preibisch, S., Saalfeld, S., and Tomancak, P. (2009). Globally optimal stitching of tiled 3D microscopic image acquisitions. *Bioinformatics* *25*, 1463–1465. <https://doi.org/10.1093/bioinformatics/btp184>.
 39. Saalfeld, S., Fetter, R., Cardona, A., and Tomancak, P. (2012). Elastic volume reconstruction from series of ultra-thin microscopy sections. *Nat. Methods* *9*, 717–720. <https://doi.org/10.1038/nmeth.2072>.
 40. Hörl, D., Rojas Rusak, F., Preusser, F., Tillberg, P., Randel, N., Chhetri, R.K., Cardona, A., Keller, P.J., Harz, H., Leonhardt, H., et al. (2019). BigStitcher: reconstructing high-resolution image datasets of cleared and expanded samples. *Nat. Methods* *16*, 870–874. <https://doi.org/10.1038/s41592-019-0501-0>.
 41. Lowe, D.G. (1999). Object recognition from local scale-invariant features. In Proceedings of the Seventh IEEE International Conference on Computer Vision (IEEE), 2 (IEEE), pp. 1150–1157. <https://doi.org/10.1109/ICCV.1999.790410>.
 42. Fischler, M.A., and Bolles, R.C. (1981). Random sample consensus: a paradigm for model fitting with applications to image analysis and automated cartography. *Commun. ACM* *24*, 381–395. <https://doi.org/10.1145/358669.358692>.
 43. Arun, K.S., Huang, T.S., and Blostein, S.D. (1987). Least-squares fitting of two 3-d point sets. *IEEE Trans. Pattern Anal. Mach. Intell.* *9*, 698–700. <https://doi.org/10.1109/tpami.1987.4767965>.
 44. Pentimalli, T.M., Schallenberg, S., León-Periñán, D., Legnini, I., Theurillat, I., Thomas, G., Boltengagen, A., Fritzsche, S., Nimo, J., Ruff, L., et al. (2023). High-resolution molecular atlas of a lung tumor in. Preprint at bioRxiv. <https://doi.org/10.1101/2023.05.10.539644>.
 45. Arganda-Carreras, I., Sorzano, C.O.S., Marabini, R., Carazo, J.M., Ortizde-Solorzano, C., and Kybic, J. (2006). Consistent and Elastic Registration of Histological Sections Using Vector-Spline Regularization. In *Computer Vision Approaches to Medical Image Analysis Lecture Notes in Computer Science*, R.R. Beichel and M. Sonka, eds. (Springer Berlin Heidelberg), pp. 85–95. https://doi.org/10.1007/11889762_8.
 46. Virshup, I., Rybakov, S., Theis, F.J., Angerer, P., and Wolf, F.A. (2021). anndata: Annotated data. Preprint at bioRxiv. <https://doi.org/10.1101/2021.12.16.473007>.
 47. Zeira, R., Land, M., Strzalkowski, A., and Raphael, B.J. (2022). Alignment and integration of spatial transcriptomics data. *Nat. Methods* *19*, 567–575. <https://doi.org/10.1038/s41592-022-01459-6>.
 48. Arganda-Carreras, I., Kaynig, V., Rueden, C., Eliceiri, K.W., Schindelin, J., Cardona, A., and Sebastian Seung, H. (2017). Trainable Weka Segmentation: a machine learning tool for microscopy pixel classification. *Bioinformatics* *33*, 2424–2426. <https://doi.org/10.1093/bioinformatics/btx180>.
 49. Schmidt, U., Weigert, M., Broaddus, C., and Myers, G. (2018). Cell Detection with Star-Convex Polygons. In *Medical Image Computing and Computer Assisted Intervention – MICCAI 2018*, A.F. Frangi, J.A. Schnabel, C. Davatzikos, C. Alberola-López, and G. Fichtinger, eds. (Springer International Publishing), pp. 265–273. https://doi.org/10.1007/978-3-030-00934-2_30.
 50. Stringer, C., Wang, T., Michaelos, M., and Pachitariu, M. (2021). Cellpose: a generalist algorithm for cellular segmentation. *Nat. Methods* *18*, 100–106. <https://doi.org/10.1038/s41592-020-01018-x>.
 51. Guo, L., Li, Y., Qi, Y., Huang, Z., Han, K., Liu, X., Liu, X., Xu, M., and Fan, G. (2023). VT3D: a visualization toolbox for 3D transcriptomic data. *J. Genet. Genomics* *50*, 713–719. <https://doi.org/10.1016/j.jgg.2023.04.001>.
 52. Larsson, L., Franzén, L., Ståhl, P.L., and Lundeberg, J. (2023). Semla: a versatile toolkit for spatially resolved transcriptomics analysis and visualization. *Bioinformatics* *39*, btad626. <https://doi.org/10.1093/bioinformatics/btad626>.
 53. Atta, L., Clifton, K., Anant, M., Aihara, G., and Fan, J. (2024). Gene count normalization in single-cell imaging-based spatially resolved transcriptomics. *Genome Biol.* *25*, 153. <https://doi.org/10.1186/s13059-024-03303-w>.
 54. Marin, Z., Graff, M., Barentine, A.E.S., Soeller, C., Chung, K.K.H., Fuentes, L.A., and Baddeley, D. (2021). PYMEVisualize: an open-source tool for exploring 3D super-resolution data. *Nat. Methods* *18*, 582–584. <https://doi.org/10.1038/s41592-021-01165-9>.
 55. Schaap, W.E., and van de Weygaert, R. (2000). *Continuous Fields and Discrete Samples: Reconstruction through Delaunay Tessellations*. Preprint at arXiv.

STAR★METHODS

KEY RESOURCES TABLE

REAGENT or RESOURCE	SOURCE	IDENTIFIER
Software and algorithms		
STIM	GitHub	https://doi.org/10.5281/zenodo.14911427
STIMwrap	GitHub	https://doi.org/10.5281/zenodo.14930579

METHOD DETAILS

Related software

Spacemake³⁰ is used for processing and basic visualization only; VT3D,⁵¹ Spateo Viewer,²⁵ and Vitessce¹⁵ are designed for visualization purposes only; Seurat¹⁶ and squidpy¹⁷ offer both analyzing and viewing, but 3D visualization and sections alignment are unavailable; ST Viewer¹⁸ is tailored to datasets generated with Spatial Transcriptomics⁶; histoCAT¹⁹ and Giotto Viewer²⁰ do not offer sections alignment. Semla⁵² (formerly STUtility²¹) offers a basic alignment, but requires manual registration for high-quality results.

N5 storage and normalization

STIM ingests spatial sequencing data that is stored in the AnnData standard, or as (compressed) text files containing locations and barcodes of sequenced spots, expression levels, and optionally cell type predictions per dataset. The current framework supports 2D and 3D coordinates, and can be readily extended. Initially, STIM re-saves or links the set of AnnData or text-file based datasets into a common N5 container that can be accessed as one common project, e.g. the image registration pipeline can be applied to an entire or parts of a project. By default, locations and expressions are stored with double precision and Gzip compression using a block length of 16,384 for locations and a block size of 512x512 for expression values (Figure 1B). Genes and the barcode list of each dataset together with their transformations are currently stored as metadata in the N5 container. The N5 data can be accessed in STIM/stimwrap or directly through Java and python N5 packages.

Optionally, the data can be normalized upon re-saving to N5 or at a later time. We have adopted here the standard library size normalization in log-space commonly used for scRNA-seq datasets, with the drawbacks discussed for imaging-based spatial transcriptomics datasets.⁵³ More specifically, if d_{ij} represents the raw count for gene i in spatial unit j , we normalize values as

$$d_{ij} \rightarrow d'_{ij} = \log_2 \left(10^5 \times \frac{d_{ij}}{\sum_k d_{kj}} + 1 \right)$$

where the dummy index k is used for summing over all genes within a spatial unit.

Rendering of irregularly-spaced data

Image data is typically stored in n -dimensional, integer-based Cartesian coordinate systems that are natively supported by most camera chips and display devices. In contrast, spatial sequencing data consist of measurements at arbitrary, floating-point precise locations, which stem from accurately localizing sequenced locations. To render such data, they need to be mapped to an integer-based cartesian coordinate system supported by standard display devices (e.g. to a 2048x1536 pixel grid), a problem that also occurs in other dataset types such as localization-based superresolution microscopy⁵⁴ and other disciplines such as astronomy.⁵⁵ Straight-forward, fast mapping can be achieved through nearest-neighbor interpolation using kd-trees. Resulting images are effectively Voronoi-tessellations with sharp, unnatural boundaries and artificial appearance where point densities are low towards the edges (Figures S6A and S6B). Distance-weighted interpolation creates more natural-looking images, which, however, still contain unnatural edges as either a number of points or maximal distance for interpolation needs to be defined (Figure S6C). Large values are able to create reasonable representations in areas of high point densities, but can still produce artificial structures, especially towards the edges of the dataset (Figure S6D). To overcome these issues we represent each location as a Gaussian distribution, and each pixel is rendered as the sum of all overlapping distributions, normalized by their respective weights. In order not to create hard boundaries in areas with few locations, normalization is only performed if the sum of weights is bigger than one. This mapping is fast and produces representations of the data resembling naturally-looking images that can therefore easily be processed with computer vision tools and are additionally visually pleasing (Figures 1 and S6E; Video S2).

Filtering of irregularly-spaced data

Within STIM, we implemented a framework for spatial filtering of irregularly-spaced datasets based on kd-trees. We added mean filtering, median filtering, Gaussian filtering, as well as practical filters to hide single, isolated locations and to visualize the density

of locations. Adding new filters is straight-forward, and typically requires the implementation filter.RadiusSearchFilter class, which already provides the kd-tree search and the location to be filtered.

Such basic filtering operations can for example help to smoothen noisy spatial sequencing data, to emphasize larger structures, or to identify edges (Figure 1C; Video S2).

Pairwise SIFT registration

In order to robustly identify corresponding points between pairs of two-dimensional serial sections of spatial sequencing datasets we first employ the Scale Invariant Feature Transform (SIFT) on images of renderings of individual genes.

First, we identify a set of genes (by default 100) that are expressed in both serial sections and show the highest combined standard deviations of their expression values, thus automatically selecting genes that are likely to show patterns that are helpful to perform an alignment. The user can additionally add genes that are known to create well-structured expression renderings. Second, we compute SIFT on all pairs of genes individually, using a low minimal number of corresponding points (inliers, by default 5) on a rigid model. Finally, we perform another RANSAC consensus across the points of all genes, requiring by default at least 30 inliers. This combination of parameters was very robust in our tests and worked out of the box for SlideSeq, Visium, and Open-ST datasets.

Global Optimization

In order to align more than two serial sections we first compute pairwise SIFT registrations between close-by sections (by default +-2). We then solve an optimization problem by finding a set of transformations T_V that minimize the distance between all corresponding points $C_{A,B}(g)$ of all serial sections V across all genes G by identifying.³⁸

$$\arg \min_{T_V} \sum_{A \in V} \left(\sum_{B \in V \setminus A} \left(\sum_{g \in G} \left(\sum_{(a,b) \in C_{A,B}(g)} \|R_A \underline{a} - R_B \underline{b}\| \right) \right) \right)$$

Finally, wrong pairs of correspondences $C_{A,B}(g)$ can be identified and removed by iteratively analyzing inconsistencies between pairwise results and the current state of the global optimization as defined by the current set of transformations T_V .⁴⁰ By default we employ rigidly regularized ($\alpha = 0.1$) affine transformation models T_V for each serial section in the optimization process. All transformations are stored within the N5 metadata, thus all visualization tools of STIM will directly use these transformations.

ICP refinement

After global optimization based on the corresponding interest points identified by SIFT we optionally employ Iterative Closest Point (ICP) for refinement of the transformations. In contrast to the SIFT alignment step, ICP is performed on the actual coordinates of the sequenced locations. We first compute pairwise ICP's between close-by serial sections (+-2 sections) using only the expression values of genes that yielded SIFT correspondences. The basic idea of ICP is to assign nearest neighboring points as corresponding points, update the transformation based on this assignment, and iterate this procedure until convergence or a maximum number of iterations is achieved. Here, we do not simply assign nearest points to each other, but those who show the most similar expression vector in the local vicinity (by default the median distance between all sequenced locations). We optionally support RANSAC filtering on the sets of corresponding points during each ICP iteration in order to identify a consensus update vector across all neighboring points. After all pairwise ICP matchings are performed, we re-solve the global optimization problem using the corresponding points identified in the last iteration of every respective ICP run.

QUANTIFICATION AND STATISTICAL ANALYSIS

Benchmarking

To benchmark the alignment accuracy, we compare how different human experts and methods transform the same tissue sections. For any two methods A and B, we compute their pairwise transformation differences. Given a section s with points $\{p_1, \dots, p_n\}$, we measure the average distance between transformed positions:

$$\text{error}(A, B) = \frac{1}{n} \sum_i |T_A(p_i) - T_B(p_i)|$$

where T_A and T_B are the affine transformations from methods A and B computed relative to the previous section, and distances are in microns. Manual alignment was performed using interactive BDV tools, which is accessible in STIM as Manual Alignment under the "st-align-interactive" command. For both STIM and manual alignment a Similarity Model (rigid+scaling) was used.

We further performed a grid search over STIM's scale and render factor parameters, measuring each configuration's error against expert annotations.

We ran Morpho on CPU with default parameters from spateo-release version 1.1.0, with SVI_mode=True and mode='SN-S'. For computational performance reasons, data was subset to 1:5 cells, and the top-10 highly variable genes computed with scanpy 1.9.1. We ran Spacel with default parameters as of version 1.1.7, n_neighbors=15, n_threads=10, p=2, using the original cell type annotation provided for the metastatic lymph node dataset.

The other methods based on gene expression (GPSA, PASTE2) either did not run for the metastatic lymph node, or did not finish after a running time of two weeks.